symmetry

IMPACT FACTOR 2.2

CITESCORE 5.4

Article

Review on QCD Studies with the CMS Experiment

Olga Kodolova

MDPI

https://doi.org/10.3390/sym17020260

symmetry

MDPI

Article

Review on QCD Studies with the CMS Experiment

Olga Kodolova [1,2]

[1] Skobeltsyn Institute of Nuclear Physics, M.V. Lomonosov Moscow State University, 119991 Moscow, Russia; olga.kodolova@cern.ch
[2] Joint Institute for Nuclear Research, 6 Joliot-Curie St, 141980 Dubna, Russia

Abstract: The CMS experiment provides measurements of the soft and hard QCD processes using samples of proton–proton and AA collisions collected at different energies. Measurements include particle multiplicity, particle momentum spectra and correlations, jet properties and production rates, and are compared with predictions of theoretical models at leading, next-to-leading and next-next-to-leading QCD fixed order accuracy. The data in combination with measurements obtained by other experiments are used to measure the strong coupling constant and for PDF constraints.

Keywords: QCD; PDF; high energy; strong coupling constant; correlations; CMS; LHC

1. Introduction

Quantum Chromo Dynamics (QCD) is the fundamental theory of strong interactions and was developed within the framework of the standard model (SM) theory, which unifies electromagnetic, weak and strong interactions. The development commenced during the 1960s of the previous century. However, parameters of QCD theory are still not fully defined, and calculations of different processes are carried out in fixed-order series combined with phenomenological approximations, which are obtained from the experimental data received at different energies of colliding beams.

Another important finding is that processes based on pure strong interactions constitute an important background for new territory in physics searches, as due to its enormous cross-section QCD may hide many possible signals of new physics. QCD processes contribute to any measurement performed in hadron colliders. That means that QCD contributes also to the processes where an electroweak interaction is involved.

The knowledge of different QCD parameters can be achieved via detailed measurements of the production yield and characteristics of particles in both the soft and hard momentum regimes. The possibility to decouple "soft" and "hard" physics is based on the factorization property, which allows separating parton density functions (PDFs) from the hard interaction, and consequent parton showering (PS) and hadronization:

$$\sigma_{pp}(s;\alpha_S,\mu_F,\mu_R) = \sum_{a,b}\int_0^1 f_a(x_1,\mu_F,\mu_R) f_b(x_2,\mu_F,\mu_R)\hat{\sigma}^{ab->X}(s,x_1,x_2,\alpha_s,\mu_F,\mu_R) \quad (1)$$

where the strong coupling constant, parton density functions ($\alpha_s(\mu_R)$, $f(x,\mu_F,\mu_R)$) are estimated experimentally from data via the approximating procedure, and $\hat{\sigma}$ is the parton–parton cross-section at the fixed order of α_S expansion of the full cross-section. Currently, the fixed-order cross-section is calculated up to NLO accuracy and NNLO accuracy for some processes. However, the essential part of the theory model is the connection between partons produced at the production vertex at fixed order and final particles visible by the

Academic Editor: Ulf Meißner

Received: 30 December 2024
Revised: 2 February 2025
Accepted: 6 February 2025
Published: 9 February 2025

Citation: Kodolova, O. Review on QCD Studies with the CMS Experiment. *Symmetry* **2025**, *17*, 260. https://doi.org/10.3390/sym17020260

detector. To achieve the transition, the hard parton scattering from Equation (1) is followed by the parton showering (PS), fragmentation (hadronization process) and, finally, is ended with particles. The hard interaction of the parton pair (production vertex) is accompanying by multiparton scattering (MPI) that produces additional interactions among the other partons presented in the colliding protons, which provide the additional particles in the same production vertex. Most MPI processes are soft ones, but there is a non-zero probability to have one or more of the additional hard interactions. Note that these hard interactions occur in the same production vertex (double parton scattering or DPS, triple parton scattering or TPS, etc.) and, thus, two or more hard interactions cannot be distinguished by the observer (detector). The main problem for rare events searches is that NPS (N parton scattering) can mimic rare events. This means that, without the proper knowledge of the NPS, the SM background is underestimated. The next complication for different analyses comes from the instantaneous luminosity that is needed to observe rare processes, which is requested to be so high that it allows tens of additional interactions (pileup events) to occur in a single bunch crossing (pileup). These events are mostly QCD events and most of such events are soft, but it is possible that more than one hard interaction is registered due to pileup. Fortunately, these kinds of events belong to the different production vertices and can be separated by tracker measurements in the detector part covered by the tracker. Measured observables are compared with QCD calculations and hadronization models to test the validity of the theoretical ideas and to allow an improvement of the phenomenological description embedded in the calculations. Practically, measured observables are compared with theoretical calculations at the level of particles. This involves the unfolding procedure applied to the spectra measured with the detector (backward propagation from detector signal to particles), which takes into account the apparatus function of the detector. From the theory side, the partonic vertex is propagated to particles via showering and hadronization (forward propagation).

Although there are a plenty of important measurements of soft processes, the review is mainly devoted to hard QCD measurements, while a few subjects are chosen in the soft QCD field.

2. CMS Detector

The CMS apparatus is equipped with a superconducting solenoid with a diameter of 6 m, which provides a magnetic field of 3.8 T. A lead tungstate crystal electromagnetic calorimeter (ECAL), and a sampling (brass and scintillator) hadron calorimeter (HCAL) are situated within the solenoid volume. Each calorimeter is composed of a barrel and two endcap sections covering the pseudorapidity range $|\eta| < 3$. In the region $|\eta| < 1.74$, the HCAL cells have widths of 0.087 in η and 0.087 in azimuth (ϕ). For $|\eta| < 1.48$, HCAL cells are mapped to 5 × 5 arrays of ECAL crystals to form calorimeter towers, which are projected radially close to the nominal interaction point. The coverage of the towers increases progressively to a maximum of 0.174 in $\Delta\eta$ and $\Delta\phi$ in the pseudorapidity range $1.74 < |\eta| < 3.0$. The energy deposits in the ECAL crystals and HCAL cells that belong to one tower are summed to define the calorimeter tower energy. Calorimeter towers are used as input to jet finders. Two very forward Cherenkov calorimeters (HF) are located at a distance of 11 m from both sides of the detector, extending in the region $3 < |\eta| < 5$. Being in the severe radiation conditions, HF calorimeters are built with radiation-hard components (steel absorbers and quartz fibers). HF measures high energy jets via detecting Cherenkov light emitted by shower particles in the quartz fibers. To identify and measure muons, gas-ionization chambers are embedded in the steel outside the solenoid in the pseudorapidity range $|\eta| < 2.4$. Detection planes were made using three technologies: drift tubes, cathode strip chambers and resistive plate chambers. A two-tier trigger system was

designed for the CMS to suppress the event rate. Custom hardware processors are used at the first level, taking information from calorimeters and muon detectors to select events at a rate of around 100 kHz within a time interval of less than 4 µs. The high-level trigger (the second level) is performed within a farm of processors. Full event reconstruction, which is optimized for fast processing, reduces the event rate by 100 times down to 1 khz.

The detailed description of the CMS detector can be found in Ref. [1].

3. QCD Measurements

The CMS program includes both soft and hard processes studies. Moreover, without detailed knowledge of soft interactions, it may not be possible to describe the hadronization process and underlying event that contribute to jets and missing-p_T measurements, and, subsequently, to estimate parton distribution functions, α_S, etc.

3.1. Soft and Semihard QCD

3.1.1. Multiplicity and Scales

Charge particle density in the mid-rapidity region is connected proportionally to the gluon density at the production vertex, which in turn reflects the interplay between soft and hard processes. However, there is no possibility to measure the very low transverse momentum of charged particles in the detector. Usually, the multiplicity of charge particles is estimated with some cuts on the transverse momentum of the particle. Then, the multiplicity value can be extrapolated to the multiplicity of particles with $p_T > 0$ GeV, assuming some physics model. CMS measurements are performed with the cut on the transverse momentum of 500 MeV, and give a particle density equal to three particles per rapidity unit at a colliding energy of 13 TeV in the mid-rapidity region in the fiducial volume [2], as shown in Figure 1 (left).

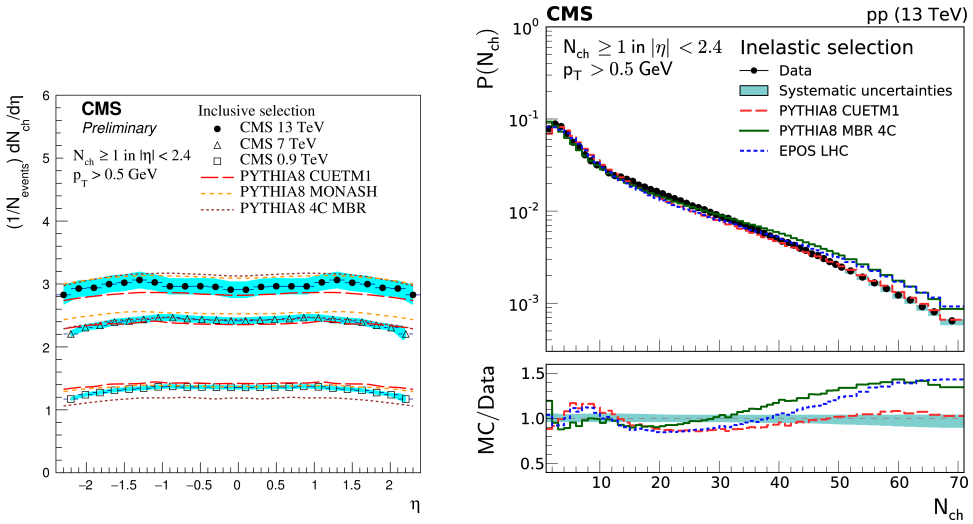

Figure 1. (**Left**): Charged particle pseudorapidity distribution for the inclusive event sample at $\sqrt{s} = 900$ GeV, 7 TeV and 13 TeV. The total systematic uncertainty is presented as a shaded band. Predictions of of the MC generators PYTHIA 8 with the tunes Monash and CUETP8M1, PYTHIA 8 MBR with the tune 4C, HERWIG++ with the tune UE-EE-4C, and EPOS with the LHC tune are shown with lines of different styles. (**Right**): Charged particle multiplicity distributions of the inelastic event sample. Predictions of of the MC generators PYTHIA 8 CUETM1 (long dashes), PYTHIA 8 MBR4C (continuous line), and EPOS LHC (short dashes) are shown. The total systematic uncertainty is presented as a shaded band. The corresponding MC-to-data ratios are shown in lower panel.

After propagation to the transverse momentum of zero, the particle density approaches 5.49, which is in good agreement for CMS, ATLAS and ALICE observations [3–5]. At LHC

energy, a slope around n = 20 is observed [6] and a well-pronounced multicomponent structure starts to be clearly visible in multiplicity distribution, as presented in Figure 1 (right). The multicomponent structure of the multiplicity distribution is sensitive to multiparton interactions and was firstly observed at CERN SPS [7]. The important feature observed in particle production is the existence of dependencies that can be scaled with respect to collision energy, e.g., the rise of the mean transverse momentum as a function of charged particles multiplicity is energy independent, the production of forward particles is independent on collision energy, and the phase-space invariant yield, Ed^3N_{ch}/dp^3, as a function of $x_T = 2p_T/\sqrt{s}$ measured at different collision energies is consistent with pQCD predictions with the exponent equal to 4.9 [8–10].

3.1.2. Ridge Effect

One of the most powerful observables to manifest the collision dynamics is the correlation measurements. In particular, experiments provided the measurement of dihadron azimuthal correlations to study the properties of the strongly interacting medium created in ultrarelativistic nuclear collisions. Firstly, the long-range correlations (ridge) were observed in experiments at RICH [11,12], and were considered as the feature of high-energy heavy ion collisions only. It was considered that the collective effect resulted either from the interaction of high-p_T partons with dense matter [13] or being the interrelation between jet quenching and hydrodynamical transverse flow [14]. At LHC energies (7–14 TeV), the fastly growing gluon density and increasing the number of multiparton interactions lead to the number of produced particles in central pp events approaching the number of produced particles in high-energy collisions (200 GeV/n-n) of intermediate-size nuclear (Cu-Cu) [12]. A set of theoretical papers predicted that some of the effects seen in nuclei–nuclei collisions may appear in proton–proton collisions at LHC energies [15–18]. In the first year of the LHC era (2010), the CMS observed a ridge effect in pp collisions at the collision energy of 7 TeV [19]. It is seen as the pronounced structure in high-multiplicity pp events (central pp events with a small impact parameter or large overlapping area) in the two-dimensional correlation function for particle pairs with the transverse momentum of 1–3 GeV/c, $2.0 < |\Delta(\eta)| < 4.8$ and $\Delta(\phi)$ near 0. This is the first observation of a long-range, near-side structure in two-particle correlation functions in pp collisions, which points to the potentially similar collective effects in pp and AA collisions. The ridge was also observed in pPb [20] and in central PbPb collisions in a nucleon–nucleon $\sqrt{s_{NN}} = 2.76$ TeV [21]. The correlations were studied over a broad range of pseudorapidity ($|\eta| < 2.4$) and over the full azimuth (ϕ) as a function of charged particle multiplicity and transverse momentum (p_T) in pp collisions at 13 TeV [22]. This appears to be similar to the ridge found in pp data at $\sqrt{s} = 7$ TeV. The results were confirmed by ATLAS and ALICE [23–26]. After the many years of the ridge observation, the nature of this effect and its similarity for pp, pPb and PbPb is still unclear, although there are some ideas that are able to describe the ridge effect qualitatively [27]: gluon saturation at small x [28], hydrodynamical evolution [29] and interacting strings [30]. Proposed interpretations of the ridge effect in pp interactions are closely connected with the description of the ridge effect in heavy ion collisions.

3.2. Hard QCD

3.2.1. Multiparton Scattering and Underlying Event

One of the important subjects is the underlying event (UE), which is everything in the event that is not connected with hard parton interaction, i.e., initial (ISR) and final (FSR) state radiation and multiparton interactions. UE activity is typically studied in the transverse, away and towards regions in pp collisions as a function of the hard scale of the event, and at different centre-of-mass energies. As the measure of hard scale, one

may consider events with a high-energy track or jet (hadronic events), Drell-Yan events and events with top–antitop quarks production [31–33]. One may consider all particles in an event or follow for the particle species. The knowledge of UE allows for better evaluation of the event hard scale. Most of UE particles are the result of the soft interactions; however, there is the non-zero probability of the additional hard interaction(s) in the same event. N-parton scattering may produce the irreducible background to rare processes. Moreover, studies of n-parton scattering (NPS) processes are important to evaluate the inner structure of the proton and its evolution with energy. Many of features, such as the various correlations between individual partons, are very difficult to calculate theoretically, and can only be estimated through experimental studies of NPS in different systems and for different numbers, N, of simultaneous scatterings. Most of the studies so far have dealt with two hard interactions in an event (DPS), which are characterized by the formula ignoring the correlations in between partons:

$$\sigma_{DPS}^{AB} = \frac{m}{2}\frac{\sigma_{SPS}^{A}\sigma_{SPS}^{B}}{\sigma_{eff,DPS}} \tag{2}$$

where $\sigma_{SPS}^{A/B}$ is the partonic vertex cross-section for A and B processes, while

$$\sigma_{eff,DPS} = \left(\int d^2b(T(b))^2\right)^{-1} \tag{3}$$

with $T(b)$—overlapping function. For the recently proposed triple parton scattering also ignoring correlations, one can use the formula as proposed in [34]:

$$\sigma_{DPS}^{AB} = \frac{m}{2}\frac{\sigma_{SPS}^{A}\sigma_{SPS}^{B}\sigma_{SPC}^{C}}{\sigma_{eff,TPS}^{2}} \tag{4}$$

where

$$\sigma_{eff,TPS} = \left(\int d^2b(T(b))^3\right)^{-1} \tag{5}$$

The first observation of DPS in the production of the same-sign WW at 13 TeV was performed on the statistics of 138 fb^{-1}, with an observed significance of 6.2 and $\sigma_{eff} = 12.2 + 2.9 - 2.2$ mb [35]. The fiducial cross-section is $6.28 \pm 0.81(stat) \pm 0.69(syst) \pm 0.37(model)$ fb and inclusive cross-section is $80.7 \pm 11.2(stat) \pm 9.5(syst) \pm 12.1(model)$ fb. DPS was also measured in four jet events [36]. However, a strong dependence of the extracted values of σ_{eff} on the model used to describe the SPS contribution is observed and the uncertainty for the cross-section estimation is consequently large. The estimation gives $\sigma_{eff} =$ 7–35 mb and $\sigma_{DPS} =$ 15–70 nb. These measurements are in agreement with measurements performed in other experiments. The CMS also estimated DPS for Z + jet events, which gives the possibility to further constrain MPI models [37].

Recently, the CMS proved the existence of the TPS, registering three J/ψ resonances in one event [38]. The observation was performed at $\sqrt{s} = 13$ TeV in the two muons decay channel of the J/ψ resonance, with a statistical significance exceeded five standard deviations. The measured inclusive fiducial cross-section is estimated as $272 + 141 - 104(stat) \pm 17(syst)$ fb. Measurements are compared with theoretical expectations for triple-J/ψ meson production in single-, double- and triple-parton scattering scenarios. Double- and triple-parton scattering are the dominant contributions in the channel, assuming factorization of multiple hard-scattering probabilities. Thus, this process can be considered as the best for the observation of DPS and TPS.

3.2.2. Parton Distribution Function and α_S Measurement

One of the important requirements for QCD calculations is the knowledge of the parton distribution function for each parton species and the knowledge of α_S behaviour as a function of the scale (Q^2). According to QCD theory, the renormalization group equation is used to evaluate α_S at a different scale, Q^2, using fixed a PDF set, while PDFs are propagated to a particular scale, Q^2, via evolution equations (DGLAP, BFKL, CCFM, ...), and depend on $\alpha_S(Q^2)$. In other words, the estimation of PDFs and α_S is strongly correlated and also depends on the choice of the evolution equation. Three approaches are used to approximate PDFs and α_S: (i) define PDFs at fixed α_S, (ii) define α_S at fixed PDF set, which gives the best approximation of the Data by Theory, and (iii) combined fit of PDFs and α_S. The estimation of PDFs and $\alpha_S(Q^2)$ is performed using the fit procedure of single-, double- and triple-differential cross-sections of different processes and at different energies with the theoretical calculations included in the special package XFitter [39]. The sensitivity of analysis to a particular PDF depends also on the choice of physics process. For instance, W mass measurement is sensitive to valence quarks, W+c is sensitive to s-quark PDF, inclusive jets, multijets to gluon PDF, Z + c and Z + b processes are sensitive to c- and b-quarks PDF, etc. The selected examples of the PDFs and α_S estimation are presented below.

The double-differential cross-sections are obtained at $\sqrt{s} = 13$ TeV as a function of the jet transverse momentum, p_T , and the absolute jet rapidity, $|y|$ [40,41]. Jets are reconstructed with the anti-k_T clustering algorithm with a distance parameter of 0.4 (0.7) in $\eta - \phi$ space. The available jet p_T and the rapidity, y, range is from 97 GeV up to 3.1 TeV and $|y| < 2.0$. Collected data correspond to an integrated luminosity of 36.3 fb^{-1}. Predictions of pQCD at NNLO and at NLO with the NLL resummation correction using various sets of PDFs are compared with the measured jet cross-sections. The combination of measured jet cross-sections reconstructed with R = 0.7 at $\sqrt{s} = 13$ TeV, $t\bar{t}$ production measurements and HERA measurements of the deep inelastic scattering is used to estimate the impact of the measurements on PDFs and α_S extraction (Figure 2).

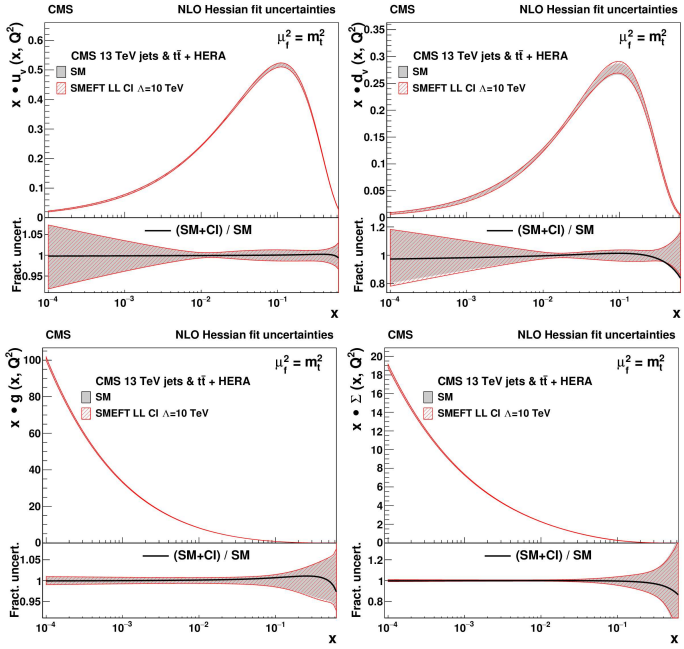

Figure 2. The u-valence (**upper left**), d-valence (**upper right**), gluon (**lower left**) and sea quark (**lower right**) distributions, resulting from the fit without and with CI terms as a function of x at the scale $\mu_f^2 = m_t^2$. The SMEFT fit is performed with the left-handed CI model with $\Lambda = 10$ TeV.

For the first time, the value of the strong coupling constant at the Z boson mass is extracted in a QCD analysis at NNLO accuracy with the inclusive jet cross-sections in proton–proton collisions. The estimated $\alpha_S(M_Z)$ is $0.1166 \pm 0.0014(fit) \pm 0.0007(model) \pm 0.0004(scale) \pm 0.0001(param.)$. In addition, the QCD analysis was performed at NLO accuracy, where jet production was combined with the normalized triple-differential top quark–antiquark production cross-section measurements. The PDFs, α_S and m_{pole} were extracted simultaneously. For the first time, a standard model effective field theory (SMEFT) analysis [42] at NLO was included in the fitting procedure over the same data, and parton distributions, together with the QCD parameters, were extracted simultaneously with imposed constraints on the Wilson coefficient, c_1, of 4-quark contact interactions. The results are comparable with the standard model. A 95% confidence level exclusion limit for the left-handed model with constructive interference, corresponding to $\Lambda > 24$ TeV, is obtained. For the first time, the interpretation of measurements is performed, taking into account the possible bias in PDFs due to physics beyond the standard model.

Correlations measurements (azimuthal angle between jets, N + 1 over N jets ratio, etc.) can be also used to estimate $\alpha_S(Q^2)$ dependence. Correlations are important as a precision test of QCD at large scales and as a test for new physics, taking into account that the new colored fermions introduce modifications to the QCD β-function [43,44].

The CMS experiment utilized a ratio observable (6), where n is the number of neighboring jets using 136 fb^{-1} of data:

$$R_{\Delta\phi}(p_T) = \frac{\sum_n nN(p_T, n)}{\sum_n N(p_T, n)} \tag{6}$$

is measured as a function of the jet transverse momentum, p_T, in events with more than or equal to three jets [45]. Basing on a comparison of the measured $R_{\Delta\phi}(p_T)$ distribution with the theoretical predictions fixing the PDF set to NNPDF3.1 NLO, the strong coupling at the scale of the Z boson mass is $0.1177 + 0.0117 - 0.0074$. The running of $\alpha_S(m_Z)$ in the TeV region does not show any deviation from the expected NLO pQCD behavior.

Extraction of PDFs for s-, c- and b-quarks is a complicated task from the reconstruction point of view as it requires the use of a special tagging procedure to identify c- and b-quarks. As it is pointed out above, to extract s-quark PDFs one may use the process W + c.

The CMS starts to study W + c production at different collision energies [46–48]. The W + c production is characterized by asymmetry of $s + \bar{s}$ production:

$$R_S = \frac{s + \bar{s}}{\bar{u} + \bar{d}} \tag{7}$$

and

$$R_c^{\pm} = \frac{\sigma(W^+ + c)}{\sigma(W^- + c)} \tag{8}$$

The associated production of a W boson with a charm quark (W + c) in pp collisions at $\sqrt{s} = 13$ TeV is studied with a data sample corresponding to an integrated luminosity of 136 fb^{-1}. The W + c process is selected based on the presence of a high transverse momentum electron or muon and a jet identified as initiated by c-quark. The c-jet signature is identified either by the presence of a muon inside a jet or by reconstructing a secondary decay vertex within the jet applying some mass constraints (c-jet tagging). The c-tagging is the most complicated task as the essential fraction of jets initiated by b-quarks is left in the sample. Taking into account the complexity of the general c-tagging, one may reconstruct the secondary vertex with the requirement of the particular mass ranges for D*-mesons. The CMS experiment uses the general c-tagger (muon and secondary vertex charm identification channels), and combines electron and muon W boson decay chan-

nels and missing transverse momentum to identify events with W decay. The measured $\sigma(W^+ + c)/\sigma(W^- + c)$ cross-section ratio is $0.95 \pm 0.005(stat) \pm 0.010(syst)$. The measurements are compared with theoretical predictions. The predicted fiducial cross-section is generally higher (up to around 10%) than the measured one, and modest deviations are observed in the shapes of the differential cross-sections. These measurements should improve the modeling of the strange quark parton distribution function.

The extraction of the c-quark PDF using the Z + c-jet production mechanism is a complicated task by the same reason, which is the contamination of b-jets in the selected c-jets sample. The first step to touch c-PDFs is to measure differential cross-sections for inclusive Z + c-jet production with respect to the transverse momentum of the Z boson and the c-jet. These measurements were carried out by the CMS in pp collisions at $\sqrt{s} = 13$ TeV with the integrated luminosity 36 fb^{-1} [49]. The measurements were performed in a fiducial space defined as: a c-jet with $p_T > 30$ GeV and $|\eta| < 2.4$, a pair of leptons with $p_T > 26$ GeV for leading lepton, and $p_T > 10$ GeV for subleading lepton and $|\eta| < 2.4$; an invariant mass of the two leptons should be between 71 and 111 GeV. The main backgrounds for Z + c-jet are Z + light jet, Z + b- jet, $t\bar{t}$ pairs and dibosons production. Unfolding of measured distributions was performed to take into account detector effects. The inclusive fiducial cross-section value for Z + c-jet production with Z $p_T < 300$ GeV was estimated as $413.5 \pm 5.6(stat) \pm 19.5(exp) \pm 5.9(th)$ pb. MADGRAPH5 aMC@NLO at NLO predicted $524.9 \pm 11.7(th)$ pb for the same fiducial volume, overestimating the measured cross-section value. SHERPA tends also to overestimate the cross-section value, while, at the same time, the prediction from MADGRAPH5 aMC@NLO at leading order shows better agreement with data than both MADGRAPH5 aMC@NLO at NLO and SHERPA.

In pQCD, the amplitude for the $Z+ >= b$-jet process can be computed using two alternative approaches: four-flavor scheme (4FS) and five- flavor scheme (5FS). In the 4FS scheme, the non-zero b-quark mass is included in the predictions, and acts as an infrared cut-off, partly removing possible divergences in the matrix element calculation, and no b-quark parton density function is used. In the 4FS scheme, the b-quark is produced by the gluon-splitting $g- > b\bar{b}$ process, while in the 5FS scheme the gluon-splitting contribution is included within a b-parton density function, and the b-quark mass is set to zero in the matrix element.

The CMS provides the extensive studies of Z + b-jet measurements [50] using the full Run2 dataset (137 fb^{-1}). The measurements are performed using the electron and muon decay modes of the Z boson in a fiducial phase space, which is defined as:

- The Z boson candidate is reconstructed from two same flavor leptons with opposite charges, requiring the invariant mass to be 71–111 GeV.
- Leading and subleading leptons have $p_T > 35$ GeV and $p_T > 25$ GeV, correspondingly.
- At least one b-jet with a tight b-tag discriminator requirement is selected, with $p_T > 30$ GeV and $|\eta| < 2.4$.
- $\Delta R > 0.4$ in $\eta - \phi$ space is required between the direction of the lepton from Z boson decay and b-jet.

The fiducial cross-sections in the combined channel are evaluated as $6.52 \pm 0.04(stat) \pm 0.40(syst) \pm 0.14(theo)$ pb for the $Z+ \geq 1$ b-jet and $0.65 \pm 0.03(stat) \pm 0.07(syst) \pm 0.02(theo)$ pb for $Z+ \geq 2$ b-jets. The measured ratios of integrated and differential cross-sections for $Z+ \geq 2$ b-jets and $Z+ \geq 1$ b-jet channels are estimated as $0.100 \pm 0.005(stat) \pm 0.007(syst) \pm 0.003(theo)$. The measurements are compared with predictions from a variety of Monte Carlo generators normalized to the inclusive Z + jets NNLO cross-section. As the conclusion, data are better described by the aMC@NLO LO simulation but overestimated by aMC@NLO NLO and SHERPA predictions (Figure 3). These are the first measurements performed for Z + b-jets at $\sqrt{s} = 13$ TeV

with large statistics. The measured cross-sections are the input for improving theoretical predictions of Z production in association with b-quarks, allowing better understanding of perturbative QCD at LO and NLO accuracy.

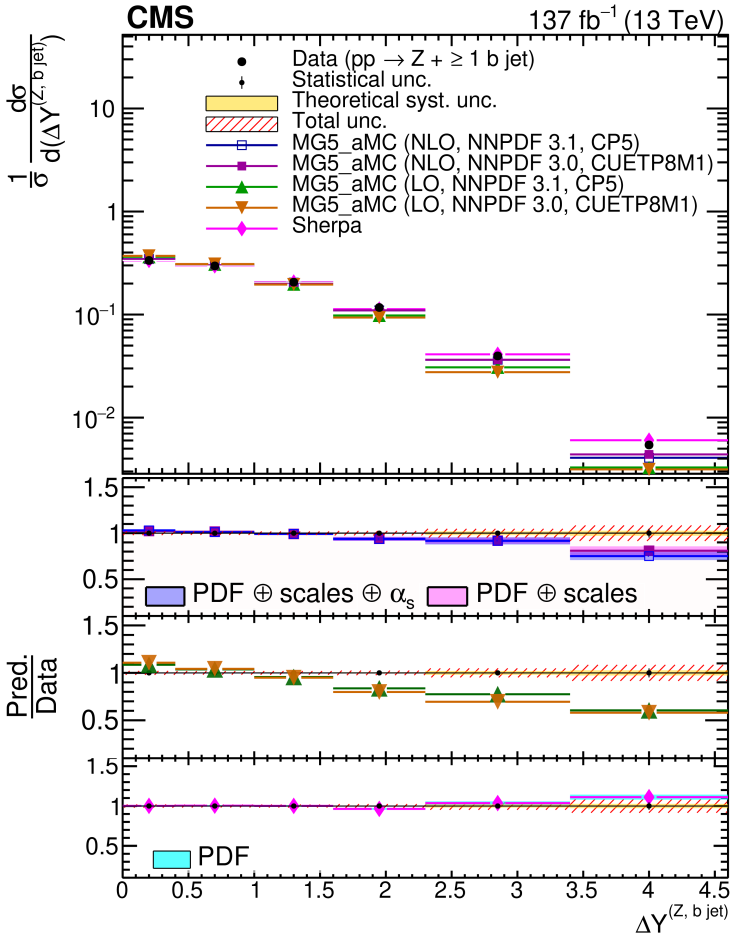

Figure 3. Normalized differential cross-section distribution as a function of $\Delta y(Z, bjet)$ between the Z boson and the leading b-jet for the Z+ $\geq$ 1 b-jet events.

3.2.3. Parton Fragmentation

The next quite new and important subject is the process of the fragmentation of quarks and gluons into color-neutral hadrons. In QCD, the emission of gluon is approximately uniform in the two-dimensional space, defined as a function of the momentum fraction of the emitted gluon with respect to the primary quark or gluon, z, and its emission opening angle, θ. This space ($ln(1/z)$, $ln(1/\theta)$) is called the Lund plane [51]. The method is applicable to jets, and analogs of Lund plane with jets (Lund Jet Plane or LJP) can be constructed [52] and, thus, can be measured. Following the proposal, the jet is found using any jet finder algorithm, and then the reconstruction is repeated using the C/A algorithm [53], which keeps an angle-ordered hierarchy of the clustering history. Then, the C/A history is reversed, starting from the hardest protojet. At each reverse step in the sequence, two observables ($ln(1/z)$, $ln(R/\Delta R)$) are created, where $z = p_T^{emission}/(p_T^{emission} + p_T^{core})$ and $\Delta R^2 = (y_{emission} - y_{core})^2 + (\phi_{emission} - \phi_{core})^2$, and p_T is the transverse momentum, y is rapidity, R is the jet radius parameter and ΔR is the angular separation of the emitted parton and parton-initiator. Observables for the Lund plane can be also chosen as $k_T = p_T^{emission} * \Delta R(p_T^{emission}, p_T^{core})$ and $ln(1/\Delta R)$. Each jet is represented by the set of points on the Lund plane. The CMS measures the LJP [54] and provide the comparison of the emission density with a set of Monte Carlo generators and theoretical calculations,

which differ in their implementation of color coherence in the parton showers and their logarithmic accuracy in different regions of the LJP, in the modeling of the UE activity and hadronization effects. Using the ability of the LJP to factorize the different compartments of physical effects (soft, hard collinear emissions, UE/MPI, ISR, hadronization fill different parts of plane), these measurements can be used to improve physics modeling of the different theoretical parts.

3.2.4. Multijet Production

Theoretical predictions for multijet events are constructed using a matrix element (ME) expansion to a fixed α_S order, followed by the parton shower (PS) approximating higher-order perturbative contributions. The ME expansion is limited to final states with less than O(10) partons and includes color correlations between quarks and gluons, and kinematic correlations between the partons. The PS may simulate multiparton final states, but probabilities are calculated with the approximations of soft and collinear kinematics, and partial or averaged color structures. In addition, MPI and hadronization provide the essential contribution in angular correlations between jets. Two kinematic variables are introduced [55] to quantify the gluon radiation pattern in multijet events: (i) the transverse momentum ratio (p_{T3}/p_{T2}) of two jets, and (ii) their angular separation (ΔR_{23}) to distinguish between soft ($p_{T3}/p_{T2} < 0.3$) and hard ($p_{T3}/p_{T2} > 0.6$) radiation, and small-angle ($\Delta R_{23} < 1$) and large-angle $\Delta R_{23} > 1$ radiation types. According to these classifications, one may consider that the events in the soft and small-angle radiation region should be well described by the PS scheme. The events in the hard and large-angle radiation region can depend on the ME scheme. The events with soft and large-angle radiation or with hard and small-angle radiation should be sensitive to both ME and PS. Events with three or more high p_T jets and inclusive Z + two-jet events are analyzed at $\sqrt{s} = 8$ TeV, corresponding to an integrated luminosity of 19.8 fb^{-1}. Three-jet events at $\sqrt{s} = 13$ TeV, corresponding to an integrated luminosity of 2.3 fb^{-1}, are added to the analysis to study the energy dependence of the radiation patterns. However, no significant dependence on the center-of-mass energy is observed in the differential distributions for three-jets events. Three-jet events are selected with the next requirements: $p_T^{j1} > 510$ GeV, $p_T^{j2/j3} > 30$ GeV, $2.14 < \Delta\phi(j1, j2) < \pi$. Z + 2 jet events are considered with $p_T^{j1} > 80$ GeV (Z is labeled as j1 in the paper), $p_T^{j2} > 30$ GeV, $p_T^{j3} > 20$ GeV, $2 < \Delta\phi(j1, j2) < \pi$, locating in the phase space different from the phase space occupying by three-jet events.

Differential distribution for three-jet events and for Z + 2 jet events have the different normalizations: three-jet spectra are normalized to an integral of the distribution, while Z + 2 spectra are normalized to the number of Z + 1 jet spectra that gives the possibility to estimate the rate of the j_3 in the sample. To facilitate the comparison of data with theoretical predictions, the data are unfolded from detector level to stable particle level, so as to remove measurement effects and to determine the true distribution of the observables. Results corrected to stable particle level are compared with several theoretical predictions at LO and NLO accuracy using different event generators (aMC@NLO LO, aMC@NLO NLO, SHERPA, POWHEG) with different numbers of partons considered in the ME. For three-jet events, it appears that wide-angle radiation and hard radiation are well described by the ME calculations, while the PS approaches fail to describe the wide-angle and hard radiation regions. The collinear region is well described by PS calculations while the ME calculations show deviations from data. In the soft region, the PS approaches describe the measurement also in the wide-angle region, while for hard radiation higher-order ME contributions are needed in the multijet measurement. The shapes of Z + 2 jet distributions are reasonably well described by all of the generators used in the analysis but the underestimation of the j_3 rate is observed for the hard emission both in collinear and wide-angle regions for all of

the generators used for the comparison. This discrepancy can be partially covered by the $t\bar{t}$ and dibosons production. The results clearly indicate that the methods of merging the ME with PS calculations are not yet optimal for describing the full region of phase space.

4. Discussion

This paper presents an overview of different measurements in the field of QCD. There are a set of experimental difficulties that almost each analysis meets in the hadronic collider. Some of them are mentioned above, such as pileup, MPI and heavy quarks tagging. However, one of the real features of the hadronic collider is that each of the hard processes may have jets in the final state due to initial state radiation. Processes that naturally have jets, i.e., quarks or gluons, in the matrix element may have the additional jets due to final-state radiation. That means that it is not easy to understand what kind of processes, 2 to 2, 2 to 3 or 2 to 4, occur at the production vertex. Another difficulty is in the definition of jet. A q-jet may be fully collected in the radius 0.5 in $\eta - \phi$-space, while for the gluon jet the radius can be spread up to 1. Jets may appear to be close to each other, and are recovered by jet splitting–merging algorithms, which include the additional ambiguity in the number of jets in the event and in the jet shape. In addition, at the level of the detector, jet energy in the calorimeter may not be correctly measured due-to non-linearity of calorimeters with respect to the hadrons, strong magnetic field, technology gaps, material in front of the calorimeter and so on. To improve the jet energy scale and jet energy resolution, the CMS created two algorithms that use the combination of tracker and calorimeter [56,57]. However, the additional jet calibration is still needed, especially taking into account the fact that only part of the calorimeters is covered by the tracker. Thus, when we talk about jets we should identify what algorithm is used for jet reconstruction, including the splitting–merging procedure, the size of the jet, and what detector or detector combination is used. In turn, reconstruction efficiency and energy scale and resolution of high-p_T objects affect the quality of the missing-p_T reconstruction and contribute into the systematics uncertainty.

Each measurement presented above is carefully studied. Systematics errors are estimated from the control samples and are described in detail in each of the cited papers.

The CMS measures both hard and soft QCD processes in various phase space regions. Measurements are compared with a wide range of LO, NLO and NNLO calculations and underlying events tunes. The CMS QCD results are used for the combinations with other experiments in global fits and in Monte Carlo models tuning. Validation of the QCD predictions (scaling properties, particles spectra, strong coupling behavior, PDFs, evolution, etc.) allows us to further constrain and tune existing models.

More results can be found on the CMS public web pages: http://cms-results.web.cern.ch/cms-results/public-results/publications/SMP/index.html (accessed on 29 December 2024), http://cms-results.web.cern.ch/cms-results/public-results/publications/FSQ/index.html (accessed on 29 December 2024).

Funding: The current review was funded by Skobeltsyn Institute of Nuclear Physics, M.V.Lomonosov Moscow State University, Russia and Joint Institute of Nuclear Research, Russia.

Data Availability Statement: The datasets presented in this article are not readily available because the data are part of an ongoing studies. Requests to access the datasets should be directed to CMS Collaboration. However, part of data can be available through CMS Open access data https://cms-opendata-guide.web.cern.ch/ (accessed on 29 December 2024).

Acknowledgments: The author acknowledges colleagues from the CMS experiment for help with collecting material for review.

Conflicts of Interest: The author declares no conflicts of interest.

Abbreviations

The following abbreviations are used in this manuscript:

MDPI	Multidisciplinary Digital Publishing Institute
DOAJ	Directory of open access journals
TLA	Three letter acronym
LD	Linear dichroism

References

1. CMS Collaboration. The CMS experiment at the CERN LHC. *J. Instrum.* **2008**, *3*, S08004.
2. CMS Collaboration. Measurement of Pseudorapidity Distributions of Charged Particles in Proton-Proton Collisions at $\sqrt{s} = 13$ TeV. CMS-PAS-FSQ-15-008, (2015), CMS Public Note. Available online: https://cds.cern.ch/record/2145373?ln=en (accessed on: 29 December 2024).
3. CMS Collaboration. Pseudorapidity distribution of charged hadrons in proton-proton collisions at $\sqrt{(s)} = 13$ TeV. *Phys. Lett. B* **2015**, *751*, 143–163. [CrossRef]
4. ATLAS Collaboration. Charged-particle distributions at low transverse momentum in $\sqrt{s} = 13$ TeV pp interactions measured with the ATLAS detector at the LHC. *Eur. Phys. J. C* **2016**, *76*, 502. [CrossRef] [PubMed]
5. ALICE Collaboration. Pseudorapidity distributions of charged particles as a function of mid- and forward rapidity multiplicities in pp collisions at $\sqrt{s}$ = 5.02, 7 and 13 TeV. *Eur. Phys. J. C* **2021**, *81*, 630. [CrossRef]
6. CMS Collaboration. Measurement of charged particle spectra in minimum-bias events from proton–proton collisions at $\sqrt{s}$ = 13 TeV. *Eur. Phys. J. C* **2018**, *78*, 697. [CrossRef]
7. Nygaard, C. Charged Particle Multiplicity Distributions into Forward Pseudorapidities in pp and PbPb Collisions at the LHC. Doctoral Thesis, University of Copenhagen, Copenhagen, Danmark, 2011.
8. CMS Collaboration. Charged particle transverse momentum spectra in pp collisions at $\sqrt{s}$ = 0.9 and 7 TeV. *J. High Energy Phys.* **2011**, *2011*, 86. [CrossRef]
9. CMS Collaboration. Charged particle multiplicities in pp interactions at $\sqrt{s}$ = 0.9, 2.36 and 7 TeV. *J. High Energy Phys.* **2011**, *2011*, 79. [CrossRef]
10. CMS Collaboration. Measurement of the energy density as a function of pseudorapidity in proton-proton collisions at $\sqrt{s}$ = 13 TeV. *Eur. Phys. J. C* **2019**, *79*, 391. [CrossRef]
11. PHOBOS Collaboration. High Transverse Momentum Triggered Correlations over a Large Pseudorapidity Acceptance in Au +Au Collisions at $\sqrt{s_{NN}}$ = 200 GeV. *Phys. Rev. Lett.* **2010**, *104*, 062301. [CrossRef]
12. STAR Collaboration. Three-Particle Coincidence of the Long Range Pseudorapidity Correlation in High Energy Nucleus-Nucleus Collisions. *Phys. Rev. Lett.* **2010**, *105*, 022301. [CrossRef]
13. Armesto, N.; Salgado, C.A.; Wiedemann, U.A. Measuring the Collective Flow with Jets. *Phys. Rev. Lett.* **2004**, *93*, 242301. [CrossRef] [PubMed]
14. Shuryak, E.V. Origin of the "ridge" phenomenon induced by jets in heavy ion collisions. *Phys. Rev. C* **2007**, *76*, 047901. [CrossRef]
15. Prasad, S.K.; Roy, V.; Chattopadhyay, S.; Chaudhuri, A.K. Elliptic flow (v2) in pp Collisions at LHC Energy: A Hydrodynamical Approach. *arXiv* **2009**, arXiv:0910.4844.
16. Bozek, P. Observation of the Collective flow in Proton-Proton Collisions. *Acta Phys. Pol. B* **2010**, *41*, 837.
17. Ortona, G.; Denicol, G.S.; Mota, P.; Kodama, T. Elliptic Flow in High Multiplicity Proton-Proton Collisions at $\sqrt{s}$ = 14 TeV as a Signature of Deconfinement and Quantum Energy Density Fluctuations. *arXiv* **2009**, arXiv:0911.5158.
18. d'Enterria, D.; Eyyubova, G.K.; Korotkikh, V.L.; Lokhtin, I.P.; Petrushanko, S.V.; Sarycheva, L.I.; Snigirev, A.M. Estimates of Hadron Azimuthal Anisotropy from Multiparton Interactions in Proton-Proton Collisions at $\sqrt{s}$ = 14 TeV. *Eur. Phys. J. C* **2010**, *66*, 173. [CrossRef]
19. CMS Collaboration. Observation of long-range, near-side angular correlations in proton-proton collisions at the LHC. *J. High Energy Phys.* **2010**, *2010*, 91. [CrossRef]
20. CMS Collaboration. Observation of long-range near-side angular correlations in proton-lead collisions at the LHC. *Phys. Lett. B* **2013**, *718*, 795. [CrossRef]
21. CMS Collaboration. Long-range and short-range dihadron angular correlations in central PbPb collisions at a nucleon-nucleon center of mass energy of 2.76 TeV. *J. High Energy Phys.* **2011**, *2011*, 76. [CrossRef]
22. CMS Collaboration. Measurement of Long-Range Near-Side Two-Particle Angular Correlations in pp Collisions at $\sqrt{s}$ = 13 TeV. *Phys. Rev. Lett.* **2016**, *116*, 172302. [CrossRef] [PubMed]
23. ALICE Collaboration. Long- and short-range correlations and their event-scale dependence in high-multiplicity pp collisions at $\sqrt{s}$ = 13 TeV. *J. High Energy Phys.* **2021**, *2021*, 290. [CrossRef]

24. ATLAS Collaboration. Observation of Long-Range Elliptic Azimuthal Anisotropies in $\sqrt{s}$ = 13 and 2.76 TeV pp Collisions with the ATLAS Detector. *Phys. Rev. Lett.* **2016**, *116*, 172301.
25. ALICE Collaboration. Emergence of Long-Range Angular Correlations in Low-Multiplicity Proton-Proton Collisions. *Phys. Rev. Lett.* **2024**, *132*, 172302. [CrossRef]
26. ALICE Collaboration. Measurements of long-range two-particle correlation over a wide pseudorapidity range in p–Pb collisions at $\sqrt{s_{NN}}$ = 5.02 TeV. *J. High Energy Phys.* **2024**, *2024*, 199. [CrossRef]
27. Li, W. Observation of a 'Ridge' correlation structure in high multiplicity proton-proton collisions: A brief review. *Mod. Phys. Lett. A* **2012**, *27*, 1230018. [CrossRef]
28. Venugopalan, R. The ridge through colored glass. *Nucl. Phys. A* **2014**, *931*, 277–282 [CrossRef]
29. Pierog, T.; Karpenko, I.; Katzy, J.M.; Yatsenko, E.; Werner, K. EPOS LHC: Test of collective hadronization with data measured at the CERN Large Hadron Collider. *Phys. Rev. C* **2015**, *92*, 034906. [CrossRef]
30. Bierlich, C.; Gustafson, G.; Lönnblad, L. Collectivity without plasma in hadronic collisions. *Phys. Lett. B* **2018**, *779*, 58–63. [CrossRef]
31. CMS Collaboration. Measurement of the underlying event activity in inclusive Z boson production in proton-proton collisions at $\sqrt{s}$ = 13 TeV. *J. High Energy Phys.* **2018**, *2018*, 32. [CrossRef]
32. CMS Collaboration. Study of the underlying event in top quark pair production in pp collisions at 13 TeV. *Eur. Phys. C* **2019**, *79*, 123. [CrossRef]
33. CMS Collaboration. Measurement of the underlying event activity using charged-particle jets in proton-proton collisions at $\sqrt{s}$ = 2.76 TeV. *J. High Energy Phys.* **2015**, *2015*, 137. [CrossRef]
34. d'Enterria, D.; Snigirev, A.M. Triple parton scatterings in high-energy proton-proton collisions. *Phys. Rev. Lett.* **2017**, *118*, 122001. [CrossRef] [PubMed]
35. CMS Collaboration. Observation of Same-Sign WW Production from Double Parton Scattering in Proton-Proton Collisions at $\sqrt{s}$ = 13 TeV. *Phys. Rev. Lett.* **2023**, *131*, 091803. [CrossRef] [PubMed]
36. CMS Collaboration. Measurement of double-parton scattering in inclusive production of four jets with low transverse momentum in proton-proton collisions at $\sqrt{s}$ = 13 TeV. *J. High Energy Phys.* **2022**, *2022*, 177. [CrossRef]
37. CMS Collaboration. Study of Z boson plus jets events using variables sensitive to double-parton scattering in pp collisions at 13 TeV. *J. High Energy Phys.* **2021**, *2021*, 176. [CrossRef]
38. CMS Collaboration. Observation of triple J/ψ meson production in proton-proton collisions at $\sqrt{s} = 13$ TeV. *Nat. Phys.* **2023**, *19*, 338 [CrossRef]
39. Abdolmaleki, H.; Amoroso, S.; Bertone, V.; Botje, M.; Britzger, D.; Camarda, S.; Cooper-Sarkar, A.; Fiaschi, J.; Giuli, F.; Glazov, A.; et al. xFitter: An Open Source QCD Analysis Framework. A resource and reference document for the Snowmass study. *arXiv* **2022**, arXiv:2206.12465v1.
40. CMS Collaboration. Measurement and QCD analysis of double-differential inclusive jet cross sections in proton-proton collisions at $\sqrt{s}$ = 13 TeV. *J. High Energy Phys.* **2022**, *02*, 142.
41. CMS Collaboration. Addendum to: Measurement and QCD analysis of double-differential inclusive jet cross sections in proton-proton collisions at $\sqrt{s}$ = TeV. *J. High Energy Phys.* **2022**, *12*, 35.
42. Ellis, J. SMEFT Constraints on New Physics beyond the Standard Model, Andromeda Proceedings, BSM 2021 online. *arXiv* **2021**, arXiv:2105.14942
43. Kaplan, D.E.; Schwartz, M.D. Constraining Light Colored Particles with Event Shapes. *Phys. Rev. Lett.* **2008**, *101*, 022002. [CrossRef] [PubMed]
44. Becciolini, D.; Gillioz, M.; Nardecchia, M.; Sannino, F.; Spannowsky, M. Constraining new colored matter from the ratio of 3 to 2 jets cross sections at the LHC. *Phys. Rev. D* **2015**, *91*, 015010. [CrossRef]
45. CMS Collaboration. Measurement of multijet azimuthal correlations and determination of the strong coupling in proton-proton collisions at $\sqrt{s} = 13$ TeV. *Eur. Phys. J. C* **2024**, *84*, 842. [CrossRef]
46. CMS Collaboration. Measurement of associated W + charm production in pp collisions at sqrt(s) = 7 TeV. *J. High Energy Phys.* **2014**, *2014*, 13. [CrossRef]
47. CMS Collaboration. Measurements of the associated production of a W boson and a charm quark in proton-proton collisions at $\sqrt{s}$ = 8 TeV. *Eur. Phys. J. C* **2022**, *82*, 1094. [CrossRef]
48. CMS Collaboration. Measurement of the production cross section for a W boson in association with a charm quark in proton-proton collisions at $\sqrt{s}$ = 13 TeV. *Eur. Phys. J. C* **2024**, *84*, 27. [CrossRef]
49. CMS Collaboration. Measurement of differential cross sections for Z bosons produced in association with charm jets in pp collisions at $\sqrt{s}$ = 13 TeV. *J. High Energy Phys.* **2021**, *2021*, 109. [CrossRef]
50. CMS Collaboration. Measurement of the production cross section for Z + b jets in proton-proton collisions at at $\sqrt{s}$ = 13 TeV. *Phys. Rev. D* **2022**, *105*, 092014. [CrossRef]

51. Andersson, B.; Gustafson, G.; Lönnblad, L.; Pettersson, U. Coherence effects in deep inelastic scattering. *Z. Phys. C* **1989**, *43*, 625. [CrossRef]
52. Dreyer, F.A.; Salam, G.P.; Soyez, G. The Lund jet plane. *J. High Energy Phys.* **2018**, *2018*, 64. [CrossRef]
53. Dokshitzer, Y.L.; Leder, G.D.; Moretti, S.; Webber, B.R. Better jet clustering algorithms. *J. High Energy Phys.* **1997**, *1997*, 1. [CrossRef]
54. CMS Collaboration. Measurement of the primary Lund jet plane density in proton-proton collisions at $\sqrt{s}$ = 13 TeV. *J. High Energy Phys.* **2024**, *2024*, 116. [CrossRef]
55. CMS Collaboration. Measurements of angular distance and momentum ratio distributions in three-jet and Z + two-jet final states in pp collisions. *Eur. Phys. J. C* **2021**, *81*, 852. [CrossRef] [PubMed]
56. CMS Collaboration. Particle-flow reconstruction and global event description with the CMS detector. *J. Instrum.* **2017**, *12*, P10003. [CrossRef]
57. Kodolova, O.; Vardanian, I.; Nikitenko, A.; Fano, L.; Bruno, G. Jet energy correction with charged particle tracks in CMS. *Eur. Phys. J. C* **2005**, *40*, 33–42. [CrossRef]